Supplementary Information

Wavelength-adaptive optical angular momentum recognizer via programmable soft materials

*Peizhi Sun, Xiaoqian Wang, Yifei Wang, Conglong Yuan, Dong Shen and Zhigang Zheng**

Note 1: Mechanism to guide the NLC orientation by photoalignment

Photoalignment is an excellent approach to guide the orientation of NLC directors with high resolution and regularity.[1] Not only the adverse effects such as mechanical damage, electrostatic charge, and dust contamination bothering the traditional rubbing alignment can be eliminated using the photoalignment, but also the photoaligned arrangement is flexibly erasable and rewritable. As the used polarization-sensitive photoalignment agent in our work, the sulfonic azo dye SD1 (whose chemical structure is shown in Figure S1) molecules tend to reorient their absorption oscillators perpendicular to the polarization direction of the linearly polarized UV exposure light and accordingly guide the NLC director along the oscillators.[2]

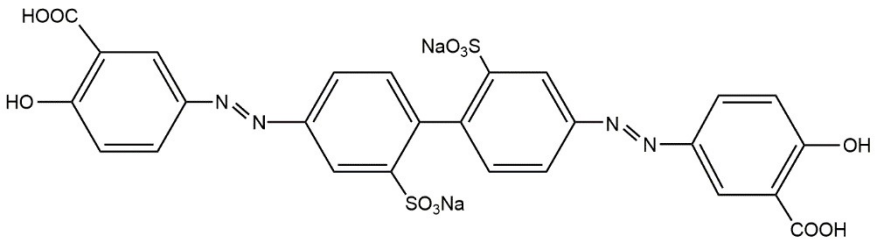

Figure S1. Chemical structure of the photoalignment agent SD1

Note 2: Mechanism of the half-wave condition to create the geometric phase in NLCs

The planar-aligned NLC we used can be characterized as a uniaxial crystal in view of optical birefringence. As passing the NLCs, the incident light E_{in} should be decomposed into two orthogonal components referring to the NLC directors, which relatively experience a birefringent phase retardation δ denoted as $\delta = 2\pi(n_{eff} - n_o)d/\lambda$, where λ is the wavelength; d is the cell gap; n_o is the ordinary refractive index and n_{eff} is the effective refractive index which gradually ranges from the extraordinary refractive

index n_e to n_o as continuously increasing the applied voltage to tilt the NLCs.[3] To be specific, for the incident light with left/right-handed circularly polarization (L/RCP) denoted as $E_{in} = [1 \quad \pm i]^{\mathrm{T}}$, the outgoing optical field E_{out} after the phase modulation of NLCs can be expressed as:[4]

$$\begin{aligned} E_{out} &= R(-\theta)\Gamma(\delta)R(\theta)E_{in} \\ &= \begin{bmatrix} \cos\theta & -\sin\theta \\ \sin\theta & \cos\theta \end{bmatrix} \begin{bmatrix} \exp(i\delta/2) & 0 \\ 0 & \exp(-i\delta/2) \end{bmatrix} \begin{bmatrix} \cos\theta & \sin\theta \\ -\sin\theta & \cos\theta \end{bmatrix} \begin{bmatrix} 1 \\ \pm i \end{bmatrix} \\ &= \cos(\delta/2) \begin{bmatrix} 1 \\ \pm i \end{bmatrix} - i\sin(\delta/2)\exp(\pm i2\theta) \begin{bmatrix} 1 \\ \mp i \end{bmatrix} \end{aligned} \tag{S1}$$

Especially, when δ reaches the half-wave condition as $\delta = (2N + 1)\pi$ where N is a random integer, E_{out} can be further rewritten as $E_{out} = \exp(\pm i2\theta)[1 \quad \mp i]^{\mathrm{T}}$, which implies the characteristic of geometric phase that the output beam is exactly transformed into the opposite circular polarization state and induced an extra phase modulation with the phase angle of $\pm 2\theta$, where θ is the azimuthal angle of NLC directors.

Note 3: Principle of designing the 3×3 NLC DVG

In our work, the proposed 3×3 NLC DVG with the phase distribution $\exp[i\psi'(x, y)]$ is characterized as a combination between the general DVG $\exp[i\psi(x, y)]$ and an additional linear phase gradient $\exp[i2k_x x]$, which can be expressed as follows:

$$\begin{aligned} \exp[i\psi'(x,y)] &= \exp[i\psi(x,y)] \cdot \exp[i2k_x x] \\ &= \sum_{N_x}\sum_{N_y} A_{N_x N_y} \exp\left[i\left(N_x k_x x + N_y k_y y\right)\right] \exp\left[i\left(N_x \Delta l_x + N_y \Delta l_y\right)\phi\right] \exp[i2k_x x] \\ &= \sum_{N_x}\sum_{N_y} A_{N_x N_y} \exp\left[i\left((N_x + 2)k_x x + N_y k_y y\right)\right] \exp\left[i\left(N_x \Delta l_x + N_y \Delta l_y\right)\phi\right] \end{aligned} \tag{S2}$$

Denote the symbol N_x' as $N_x' = N_x + 2$ and rewrite the expression of $\exp[i\psi'(x, y)]$ as:

$$\begin{aligned} \exp[i\psi'(x,y)] &= \sum_{N_x'}\sum_{N_y} A_{N_x' N_y} \exp\left[i\left(N_x' k_x x + N_y k_y y\right)\right] \exp\left[i\left((N_x' - 2)\Delta l_x + N_y \Delta l_y\right)\phi\right] \\ &= \sum_{N_x'}\sum_{N_y} A_{N_x' N_y} \exp\left[i\left(N_x' k_x x + N_y k_y y\right)\right] \left| l_{xy}' \right\rangle \end{aligned} \tag{S3}$$

where the symbol l_{xy}' is marked as $l_{xy}' = N_x' \Delta l_x + N_y \Delta l_y - 2\Delta l_x$. Notably, with $\Delta l_x = 1$ and $\Delta l_y = -3$; $N_x' \in \{+1, +2, +3\}$ and $N_y \in \{-1, 0, +1\}$, the imposed TC (l_{xy}') to the (N_x', N_y) diffraction order conforms to $l_{xy}' = N_x' - 3N_y - 2$, which enables such

NLC DVG to measure the CPOV mode of $|L\rangle|m\rangle$ ($|R\rangle|m\rangle$) with a topological charge ranging from -4 to 4.

To configure $\exp[i\psi'(x, y)]$ in our phase-only NLC element, the ideal phase distributions as $\exp[i\psi(x, y)]$ and $\exp[i2k_x x]$ are judiciously approximated from the typical binary DVG[5] and polarization grating,[6] respectively. To be specific, our proposed binary DVG is to form $\exp[i\psi(x, y)]$ with $N_x \in \{-1, 0, 1\}$ owing to $N_x = N_x' - 2$.

Notes: in the main text, to avoid too much complexity of symbols, N_x' and l_{xy}' are rewritten into N_x and l_{xy} for convenience.

Note 4: Evaluation of the broadband wavelength adaptability of such angular momentum recognizer

Beyond the proved wavelengths (λ = 532, 633, and 780 nm), the range of wavelength adaptability range can be evaluated from the voltage-transmittance (V-T) curve of a homogenous planar-aligned NLC cell which indicates the change of birefringent phase retardation δ.[7] In detail, the NLC sample is set between a pair of orthogonal polarizers, where the NLC directors are arranged at an angle of 45° to the transmission axis of either polarizer. Consequently, the transmitted light I as passing through the measuring setup can be expressed as:

$$I = I_o \sin^2(\delta/2) \tag{S4}$$

where I_o is the maximal intensity of transmitted light. We measure the transmittance of NLCs at λ = 633 nm under an applied voltage from 0 to 15 V. As shown in Figure S2, the low transmittance at high voltage (>10 V) implies an almost negligible δ, which gradually increases with the reduced voltage. According to Equation (S4), a series of peaks and valleys in the V-T curve signifies that δ reaches $m\pi$ ($m = 1, 2, 3, 4$) under the voltages of 2.3, 1.6, 1.25 and 1.0 V. From the expression of δ as $\delta = 2\pi(n_{eff} - n_o)d/\lambda$, provided both n_{eff} and n_o are constant since they are slowly changed versus λ,[8] it can be regarded that δ is inversely proportional to λ. That is, $\delta_{633\text{nm}} = 4\pi$ is equal to the relation as $\delta_{2532\text{nm}} = \pi$, referring to the half-wave condition at λ = 2532 nm. Therefore, via continuously changing the applied voltage within ΔU, the geometric-phase NLC element may dynamically work among the broad spectral

range from about 500 nm (a shorter λ may influence the photoalignment molecules) to 2500 nm, confirming the wavelength adaptability of such angular momentum recognizer in the visible and NIR band.

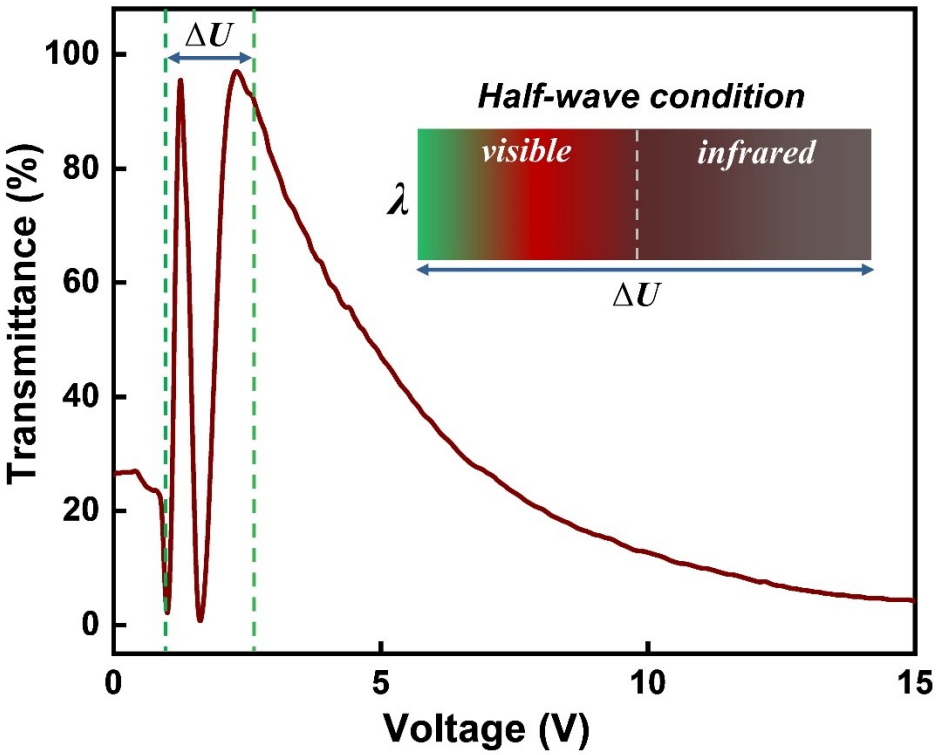

Figure S2. V-T curve of NLCs at λ = 633 nm. Inset: Wavelength adaptability from the visible to NIR band as changing the applied voltage within ΔU.

Note 5: NLC *q*-plate for generating the incident CPOV mode

In our work, the NLC-based *q*-plate, an excellent transmissive geometric phase element tremendously developed in applications such as optical communication and microscopy,[9,10] is employed to generate various CPOV beams. Generally, *q*-plate is a space-variant half-wave plate in which the optical axes acted by the NLC directors are distributed following the equation as:

$$\alpha(\phi) = q\phi + \alpha_o \tag{S5}$$

where q is the topological charge of the *q*-plate and α_o is the initial angle when $\phi = 0$, which is commonly set as zero since it does not influence the induced OAM.

The optical field modulation caused by the *q*-plate can be calculated through Jones matrix transformation.[10] In detail, the Jones matrix of the *q*-plate is written as:

$$J=\begin{bmatrix}\cos(2q\phi) & \sin(2q\phi)\\ \sin(2q\phi) & -\cos(2q\phi)\end{bmatrix} \tag{S6}$$

For a normalized LCP or RCP incident beam described as $E_{in} = (1/\sqrt{2})[1 \quad \pm i]^{\mathrm{T}}$, after passing through the *q*-plate, the output optical field E_{out} is consequently expressed as:

$$E_{out} = J \cdot E_{in} = J \cdot \frac{1}{\sqrt{2}}\begin{bmatrix}1\\ \pm i\end{bmatrix} = \frac{1}{\sqrt{2}}\exp(\pm i2q\phi)\begin{bmatrix}1\\ \mp i\end{bmatrix} \tag{S7}$$

It can be clearly observed that the transmitted beam exactly possesses the opposite circular polarization state and an additional spiral phase distribution as $\exp(\pm i2q\phi)$ is induced, which represents a CPOV mode with the topological charge *m* equal to $\pm 2q$.

Note 6: Superposition principle of CVB and CVVB

The typical complex beams as CVB and CVVB can be considered as the superposition of two independent CPOV modes. To be specific, the CVB and CVVB denoted as J_m and $J_{m,l}$, where *m* and *l* stand for the characteristic parameters, are correspondingly written as follows:

$$\begin{cases} J_m = \begin{bmatrix}\cos(m\phi)\\ \sin(m\phi)\end{bmatrix} = \frac{1}{2}\left\{e^{-im\phi}\begin{bmatrix}1\\ i\end{bmatrix} + \frac{1}{2}e^{im\phi}\begin{bmatrix}1\\ -i\end{bmatrix}\right\} = \frac{1}{2}\left\{|L\rangle|-m\rangle + |R\rangle|m\rangle\right\} \\ J_{m,l} = e^{il\phi}\begin{bmatrix}\cos(m\phi)\\ \sin(m\phi)\end{bmatrix} = \frac{1}{2}\left\{e^{i(l-m)\phi}\begin{bmatrix}1\\ i\end{bmatrix} + \frac{1}{2}e^{i(l+m)\phi}\begin{bmatrix}1\\ -i\end{bmatrix}\right\} = \frac{1}{2}\left\{|L\rangle|l-m\rangle + |R\rangle|l+m\rangle\right\} \end{cases} \tag{S8}$$

From Equation (S8), both the CVB and CVVB can be decomposed into a pair of CPOV modes with opposite circular polarization states. The difference is the pair of topological charges is exactly the opposite $\pm m$ for the CVB, while they are quantified as $l \pm m$ for the CVVB.

Note 7: Genetic algorithm optimization to design the 2×2 NLC DVG

To configure the particular 2×2 NLC DVG for encoded information processing, we propose a new scheme for design and correspondingly obtain the phase pattern via the genetic algorithm (GA) optimization process.[11] In principle, with different incident CPOV modes, the 2×2 NLC DVG should induce various diffraction vortex beam arrays with a compact spatial distribution. According to Equation (S2), a feasible configuration is set as $N_x \in \{+1, +2\}$ and $N_y \in \{0, +1\}$; $\Delta l_x = 1$ and $\Delta l_y = -2$,

which results in a consecutive range of imposed TCs (l_{xy}) from -1 to 2. To pursue an appropriate phase pattern conforming to above parameters, we revise the binary DVG into a multi-valued phase distribution with enough degrees of freedom to be optimized. To be specific, in our design of the multi-valued NLC DVG, the whole structure is decomposed into two one-dimensional vortex gratings along x and y directions, respectively. Taking the vortex grating in x direction for example, one grating period is divided into a series of subdomains, each of which refers to a specific phase. Accordingly, the amplitude coefficient (A_N) of the n-th diffraction order can be expressed as:

$$A_N = \begin{cases} \dfrac{1}{N\pi}\sum_{k=1}^{n}\exp(i\psi_{kx})\cdot\exp[-iN\pi(x_{k-1}+x_k)]\cdot\sin(N\pi\Delta x_k) & (N\neq 0) \\ \sum_{k=1}^{n}\exp(i\psi_{kx})\cdot\Delta x_k & (N=0) \end{cases} \tag{S9}$$

where n is the count of the subdomains; x_k is the transition point between the labeled k and $k + 1$ subdomains in one normalized grating period with the boundary points as $x_0 = 0$ and $x_n = 1$; ψ_{kx} corresponds to the phase of the labeled k subdomain; Δx_k is marked as $\Delta x_k = x_k - x_{k-1}$.

In our work, the genetic algorithm (GA) suitable for rapidly acquiring optimal solutions is selected in the computational process.[11] The reasonable criterion for designing the NLC DVG is to make the intensities of desired diffraction orders as high and uniform as possible. Accordingly, the merit function of genetic algorithm (GA) includes both the targets with the pair of same weights. Since $|A_N|^2$ is the intensity of n-th diffraction order, the intensity and uniformity terms of merit function can be evaluated by calculating both the sum and standard deviation of $\{|A_N|^2\}$, respectively. $\{x_k\}$ and $\{\psi_{kx}\}$ are variables to be optimized. In consequence, the phase distribution $\psi(x)$ with satisfying $\{x_k\}$ and $\{\psi_{kx}\}$ can be figured out after the optimization. Likewise, $\psi(y)$ with the optimal $\{y_k\}$ and $\{\psi_{ky}\}$ in the y direction can also be obtained. Finally, the phase distribution function $\psi(x, y)$ which realizes the expected diffraction arrays is configured by integrating $\psi(x)$ and $\psi(y)$. Notably, to acquire an eligible solution, the numbers of divided subdomains in x and y dimensions are set as six and five,

respectively. After the GA process, the optimized $\{x_k\}$, $\{\psi_{kx}\}$, $\{y_k\}$ and $\{\psi_{ky}\}$ are listed as follows:

$$\{x_k\}=\{0, 0.16, 0.324, 0.495, 0.665, 0.834,1\} \quad \| \quad \{y_k\}=\{0, 0.279, 0.451, 0.63, 0.831, 1\}$$
$$\{\psi_{kx}\}=\{4.268, 2.731, 1.173, 2.891, 1.205, 5.898\} \quad \| \quad \{\psi_{ky}\}=\{3.278, 2.535, 1.962, 4.632, 3.986\}$$

Correspondingly, to a normalized incident light, the diffraction intensities among labeled -5 ~ 5 orders from the optimized phase distribution in *x* and *y* dimensions are shown in Figure S3. For the anticipated orders as $N_x \in \{+1, +2\}$ and $N_y \in \{0, +1\}$, the diffraction intensities are {0.3245, 0.3279} and {0.3877, 0.3875}, while each intensity of remained orders are lower than 0.07, thus confirming the high efficiency and uniformity among the desired diffraction orders.

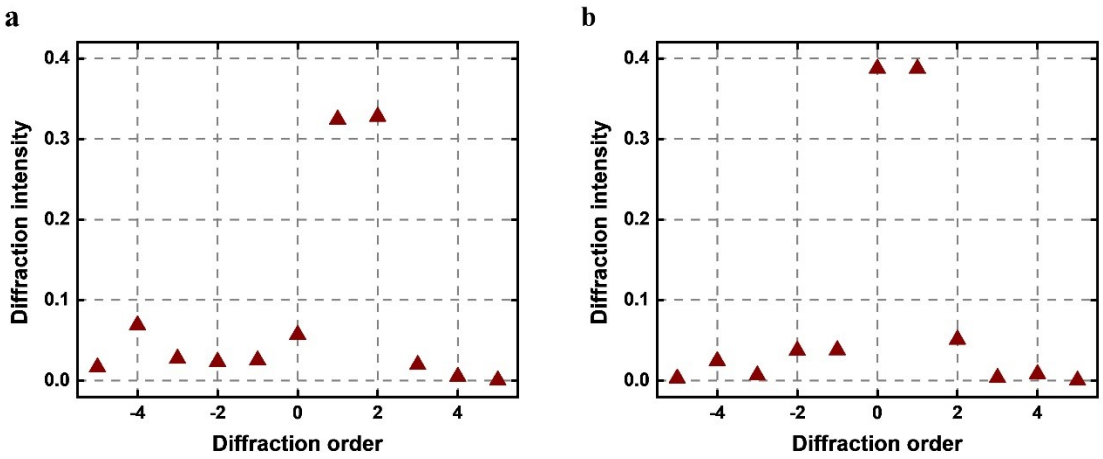

Figure S3. Intensities of diffraction orders from the proposed 2×2 NLC DVG in (a) *x* and (b) *y* dimension.

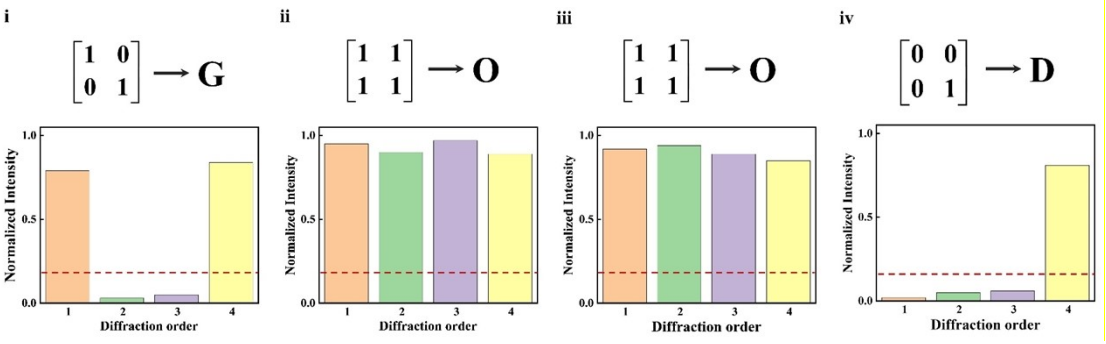

Figure S4. Measured central intensities of each diffraction orders in the superimposed diffraction array, the corresponding matrix expression and encoded English letter. The intensities are collected by a fiber spectrometer. The core diameter of optical fiber is

100 μm, which can be regarded as an aperture to filter the surrounding energy out of the fiber core. The red dashed line stands for the defined intensity threshold for binarizing the intensities into the logical '1' and '0'.

Supporting References

[1] Schadt, M., Seiberle, H. & Schuster, A. Optical patterning of multi-domain liquid-crystal displays with wide viewing angles. *Nature* **381**, 212-215 (1996).

[2] Guo, Q., Srivastava, A. K., Chigrinov, V. G. & Kwok, H. S. Polymer and azo-dye composite: a photo-alignment layer for liquid crystals. *Liq. Cryst.* **41**, 1465-1472 (2014).

[3] Hu, W. *et al.* Polarization independent liquid crystal gratings based on orthogonal photoalignments. *Appl. Phys. Lett.* **100**, 111116 (2012).

[4] Zhou, C. & Liu, L. Numerical study of Dammann array illuminators. *Appl. Opt.* **34**, 5961-5969 (1995).

[5] Zhang, N., Yuan, X. C. & Burge, R. E. Extending the detection range of optical vortices by Dammann vortex gratings. *Opt. Lett.* **35**, 3495-3497 (2010).

[6] Choi, H. *et al.* Holographic inscription of helical wavefronts in a liquid crystal polarization grating. *Appl. Phys. Lett.* **91**, 141112 (2007).

[7] Huang, C.-Y., Fung, R.-X. & Lin, Y.-G. Effects of curing conditions on electrooptical properties of polymer-stabilized liquid crystal pi cells. *Jpn. J. Appl. Phys.* **46**, 5230-5232 (2007).

[8] Wu, S. T. Birefringence dispersions of liquid crystals. *Phys. Rev. A Gen. Phys.* **33**, 1270-1274 (1986).

[9] Milione, G. *et al.* 4 x 20 Gbit/s mode division multiplexing over free space using vector modes and a q-plate mode (de)multiplexer. *Opt. Lett.* **40**, 1980-1983 (2015).

[10] Yan, L. *et al.* Q-plate enabled spectrally diverse orbital-angular-momentum conversion for stimulated emission depletion microscopy. *Optica* **2**, 900-903 (2015).

[11] Zhou, G., Chen, Y., Wang, Z. & Song, H. Genetic local search algorithm for optimization design of diffractive optical elements. *Appl. Opt.* **38**, 4281-4290 (1999).